

Intermediate spin state stabilized by the Jahn-Teller distortion in $\text{La}_{1/2}\text{Ba}_{1/2}\text{CoO}_3$ Jun Wang,^{1,2} Z. D. Wang,^{1,3} Weiyi Zhang,^{1,2} and D. Y. Xing²¹*Department of Physics, The University of Hong Kong, Pokfulam Road, Hong Kong, China*²*National Laboratory of Solid State Microstructures and Department of Physics, Nanjing University, Nanjing 210093, China*³*Texas Center for Superconductivity, University of Houston, Houston, Texas 77204*

(Received 28 March 2002; published 2 August 2002)

The recent high-resolution neutron and synchrotron diffraction measurements by Fauth *et al.* [Phys. Rev. B **65**, 060401(R) (2002)] demonstrated the existence of an intermediate spin state in half-doped $\text{La}_{1/2}\text{Ba}_{1/2}\text{CoO}_3$ which is accompanied by a long-range tetragonal Jahn-Teller distortion. In this paper we find that the charge uniform ferromagnetic intermediate spin state strongly couples to the Jahn-Teller effect and is stable only at moderate distortion of 1%. While the calculated magnetic moment of this state is in agreement with the experimentally measured one, the corresponding orbital ordering is the nearest-neighbor alternating $d_{3x^2-r^2}/d_{3y^2-r^2}$, instead of the observed uniform $d_{3z^2-r^2}$ orbital ordering. A calculation is carried out using the self-consistent unrestricted Hartree-Fock approximation on a realistic multiband d - p Hubbard Hamiltonian and a generalized Jahn-Teller coupling model, in which all possible spin-, charge-, and orbital-ordered states are considered.

DOI: 10.1103/PhysRevB.66.064406

PACS number(s): 75.25.+z, 75.30.Vn

I. INTRODUCTION

Electrons in solids carry information about spin, charge, and orbital degrees of freedom. Not all degrees of freedom are active for a given compound due to the valence state of the atoms and the crystal structure involved. In this respect, manganese-based perovskite compounds belong to a special class of materials since the interplay among spin, charge, and orbital degrees of freedom results in rich electronic and magnetic properties, among which colossal magnetoresistance is of particular importance since it has numerous applications in magnetic sensor and memory related devices.^{1,2} Similar to manganese-based perovskite compounds, cobalt-based perovskite compounds are another interesting class of materials.³⁻⁵ Because the Hund's coupling constant J_H and the crystal-field splitting $10Dq$ are very close to each other, the exact spin state of cobalt ions depends on the crystal structure, the temperature, and the divalent doping concentration. For example, the ground state of LaCoO_3 is well known to be a nonmagnetic insulator, and Co^{3+} ions take a low spin state (LS, $t_{2g}^6 e_g^0$) at low temperatures.³⁻⁸ As the temperature increases, the compound changes from a low-spin state into a paramagnetic state with a broad increase in magnetic susceptibility around 90 K. The change in magnetic properties is generally attributed to the spin-state transition of Co^{3+} ions. Up to now, there has existed a controversy concerning the high-temperature spin state: the high spin state (HS, $t_{2g}^4 e_g^2$), intermediate spin state (IS, $t_{2g}^5 e_g^1$), and a superposition of HS and LS spin states are all proposed.⁹⁻¹¹

In addition to the temperature influence, the spin state of Co ions depends also sensitively on the valence state of Co ions, which can be varied by substituting the trivalent rare-earth atoms (La) by divalent alkaline atoms such as Ba, Sr, etc. The appearance of Co^{4+} ions makes the magnetic phase diagram even more complex since charge ordering may take place. Also the existences of intermediate and high spin states makes some of these Co ions Jahn-Teller active, i.e., they can couple strongly to local lattice distortions, which in

turn affects the orbital ordering in these compounds. In fact, such phenomena were recently demonstrated by several groups through neutron-diffraction measurements. It was found that $\text{La}_{1-x}\text{Sr}_x\text{CoO}_3$ (Ref. 12) is a nonmagnetic insulator at very low Sr doping concentration, and with increasing doping the compound first changes to a spin-glass phase and then to a spin-cluster-glass phase. Eventually, when $x > 0.18$, the system becomes a ferromagnetic metal. As for the spin states of Co^{3+} and Co^{4+} ions, an earlier study conducted by Sathe *et al.*¹³ argued that Co^{3+} ions are in a mixed HS-LS state and Co^{4+} in a low spin state (LS, $t_{2g}^5 e_g^0$) in the ferromagnetic region $0.2 \leq x \leq 0.5$. Taguchi *et al.*¹⁴ also suggested that Co^{3+} ions are in a HS state for $0.5 \leq x \leq 0.9$.

Motivated by the complex phase diagram of $R_{1/2}A_{1/2}\text{MnO}_3$ (R =trivalent rare earth elements, A =divalent alkaline elements), several studies recently concentrated specifically on half doped $R_{1/2}A_{1/2}\text{CoO}_3$ compounds.¹⁵⁻¹⁷ It was found that electronic and magnetic properties depend very much on the detailed crystal structures of compounds. For small ionic radii of R ions, the large bond angle reduces the effective hopping between Co ions and induces a charge-ordering-related metal-insulator transition at low temperatures. However, for large ionic radii such as La, the crystal is nearly cubic and no charge ordering occurs.¹⁵ Similar phenomena were also observed by Troyanchuk *et al.* in their magnetization measurement,¹⁶ which indicated that the Co ions are in an IS state in $\text{La}_{1/2}\text{Ba}_{1/2}\text{CoO}_3$ and in a LS state for R with small ionic radii. Very recently, more accurate results on $\text{La}_{1/2}\text{Ba}_{1/2}\text{CoO}_3$ were unveiled by the high-resolution neutron and synchrotron powder diffraction measurement.¹⁷ This study showed that $\text{La}_{1/2}\text{Ba}_{1/2}\text{CoO}_3$ has an ideal cubic crystal structure at room temperature. The compound experiences a structural phase transition from an ideal cubic crystal to a tetragonal one, and is accompanied by a magnetic phase transition from a paramagnetic to a ferromagnetic phase when the temperature approaches $T_C \sim 180$ K. There is no charge ordering in space and the spin state is identified as the IS state. The Jahn-Teller-active IS

ions are believed to be responsible for the lattice distortion at low temperatures.

Unlike the much studied manganese based perovskite compounds $R_{1-x}A_x\text{MnO}_3$, only a few theoretical studies on cobalt-based perovskite compounds $R_{1-x}A_x\text{CoO}_3$ were done, and most of them concentrated on the undoped LaCoO_3 .⁹⁻¹¹ For the doped $\text{La}_{1-x}\text{Ba}_x\text{CoO}_3$ compounds. Zhuang *et al.*¹⁸ studied the phase diagram of various spin states as a function of doping. They applied an unrestricted Hartree-Fock approximation to a realistic multiband Hubbard model, and analyzed the relative stability of different spin states for the ideal cubic crystal structure. The HS-IS ($t_{2g}^4 e_g^{2-x} t_{2g}^{5-x} e_g^1$) nearest-neighbor ferromagnetically ordered state was found to be the most stable state for $0.41 < x < 0.95$. This result, however, is inconsistent with the very recent experimental observation that half-doped $\text{La}_{1/2}\text{Ba}_{1/2}\text{CoO}_3$ takes a charge uniform IS state rather than a HS-IS nearest-neighbor ferromagnetically ordered state. Since the IS state contains Jahn-Teller active ions and a structural phase transition is observed at low temperature, the coupling between the spin state and lattice distortion has to be taken into account.

In order to resolve the discrepancy between the current theory and experiment on the spin state in a half-doped $\text{La}_{1/2}\text{Ba}_{1/2}\text{CoO}_3$ compound, we have reinvestigated various spin states in the presence of Jahn-Teller distortion. In the absence of Jahn-Teller distortion, we find that three ferromagnetic states may become the ground state of the system in the different phase space of crystal-field splitting Dq and Hund's coupling J_H . They are the HS-IS-FM (ferromagnetic) state ($\text{Co}^{3+}\text{-HS}; \text{Co}^{4+}\text{-IS}$), the charge uniform IS-FM state ($\text{Co}^{3.5+}\text{-}t_{2g}^{4.5} e_g^1$), and the LS-LS-FM state ($\text{Co}^{3+}\text{-LS}; \text{Co}^{4+}\text{-LS}$), respectively. In the parameter range relevant to the compound, the HS-IS-FM state is found to be the ground state, being in agreement with previous calculation.¹⁸ However, the HS-IS-FM state becomes unstable when Jahn-Teller distortion is introduced, and it is replaced by a charge uniform IS-FM state. The magnetic moment of IS-FM state is also consistent with the measured magnetic moment $\sim 1.9\mu_B$. A detailed energy comparison among different Jahn-Teller distortion modes, nevertheless, shows that the Jahn-Teller distortion type with alternating $d_{3x^2-r^2}/d_{3y^2-r^2}$ orbital ordering has the lowest energy.

The rest of the paper is organized as follows. In Sec. II, we introduce the multiband d - p lattice model and the unrestricted Hartree-Fock approximation. Then the real-space recursion method is briefly outlined. In Sec. III, we present numerical results for several stable spin- and charge-ordered states, and discuss the influence of Jahn-Teller distortion on the half-doped $\text{La}_{1/2}\text{Ba}_{1/2}\text{CoO}_3$. Conclusions are drawn in Sec. IV.

II. MULTIBAND HUBBARD MODEL AND GENERALIZED JAHN-TELLER COUPLING

The multiband Hubbard model used in our calculation contains the full degeneracies of Co-3 d and O-2 p orbitals as well as on-site Coulomb repulsion and Hund's exchange interaction.¹⁹

$$\begin{aligned} \mathcal{H}_e = & \sum_{im\sigma} \varepsilon_{dm}^0 d_{im\sigma}^\dagger d_{im\sigma} + \sum_{jn\sigma} \varepsilon_p p_{jn\sigma}^\dagger p_{jn\sigma} \\ & + \sum_{ijmn\sigma} (t_{ij}^{mn} d_{im\sigma}^\dagger p_{jn\sigma} + \text{H.c.}) + \sum_{ijnn'\sigma} (t_{ij}^{nn'} p_{in\sigma}^\dagger p_{jn'\sigma} \\ & + \text{H.c.}) + \sum_{im} u d_{im\uparrow}^\dagger d_{im\downarrow}^\dagger d_{im\downarrow} d_{im\uparrow} \\ & + \frac{1}{2} \sum_{im \neq m' \sigma \sigma'} \tilde{u} d_{im\sigma}^\dagger d_{im\sigma} d_{im'\sigma'}^\dagger d_{im'\sigma'} \\ & - J_H \sum_{im\sigma\sigma'} d_{im\sigma}^\dagger \boldsymbol{\sigma} d_{im\sigma'} \cdot \mathbf{S}_{im}^d. \end{aligned} \quad (1)$$

In Eq. (1), $d_{im\sigma}$ ($d_{im\sigma}^\dagger$) and $p_{jn\sigma}$ ($p_{jn\sigma}^\dagger$) denote the annihilation (creation) operators of an electron on Co- d at site i and on O- p at site j , respectively, and ε_{dm}^0 and ε_p are their corresponding on-site energies; m and n represent the orbital index and σ denotes the spin. The crystal-field-splitting is included in ε_{dm}^0 , i.e., $\varepsilon_d(t_{2g}) = \varepsilon_d^0 - 4Dq$, $\varepsilon_d(e_g) = \varepsilon_d^0 + 6Dq$. ε_d^0 is the bare on-site energy of the d orbital. t_{ij}^{mn} and $t_{ij}^{nn'}$ are the nearest-neighbor hopping integrals for p - d and p - p orbitals, and are expressed in terms of Slater-Koster parameters ($pd\sigma$), ($pd\pi$), ($pp\sigma$), and ($pp\pi$). S_{im}^d is the total spin operator of the Co ion extracting the one in orbital m , $\tilde{u} = u - 5J_H/2$. The parameter u is related to the multiplet averaged d - d Coulomb interaction U via $u = U + (20/9)J_H$. After linearizing the above Hamiltonian using the unrestricted Hartree-Fock approximation, \mathcal{H}_e becomes

$$\begin{aligned} \mathcal{H}_e = & \sum_{im\sigma} \left[\varepsilon_{dm}^0 + u n_{im\sigma}^d - \frac{J_H}{2} \sigma (\mu_t^d - \mu_m^d) \right. \\ & \left. + \tilde{u} (n_t^d - n_m^d) \right] d_{im\sigma}^\dagger d_{im\sigma} + \sum_{jn\sigma} \varepsilon_p p_{jn\sigma}^\dagger p_{jn\sigma} \\ & + \sum_{ijmn\sigma} (t_{ij}^{mn} d_{im\sigma}^\dagger p_{jn\sigma} + \text{H.c.}) \\ & + \sum_{ijnn'\sigma} (t_{ij}^{nn'} p_{in\sigma}^\dagger p_{jn'\sigma} + \text{H.c.}). \end{aligned} \quad (2)$$

Here $n_{m\sigma}^d = \langle d_{m\sigma}^\dagger d_{m\sigma} \rangle$, $\mu_m^d = n_{m\uparrow}^d - n_{m\downarrow}^d$, and n_t^d and μ_t^d are the total electron numbers and magnetization of the Co- d orbitals. We have chosen the z axis as the spin quantization axis.

The generalized Jahn-Teller coupling between five d -orbitals and lattice distortions reads

$$\begin{aligned} \mathcal{H}_{JT} = & \sum_{i\sigma} \left\{ -g_1 Q_1(i) \sum_m d_{im\sigma}^\dagger d_{im\sigma} - g_2 \left[Q_3(i) d_{ix\sigma}^\dagger d_{ix\sigma} \right. \right. \\ & \left. \left. + \left(\frac{\sqrt{3}}{2} Q_2(i) - \frac{1}{2} Q_3(i) \right) d_{iyz\sigma}^\dagger d_{iyz\sigma} + \left(-\frac{\sqrt{3}}{2} Q_2(i) \right. \right. \right. \\ & \left. \left. - \frac{1}{2} Q_3(i) \right) d_{izx\sigma}^\dagger d_{izx\sigma} + (d_{ix^2-y^2\sigma}, d_{i3z^2-r^2\sigma}) \right. \\ & \left. \left. \times \begin{pmatrix} Q_3(i) & Q_2(i) \\ Q_2(i) & -Q_3(i) \end{pmatrix} \begin{pmatrix} d_{ix^2-y^2\sigma} \\ d_{i3z^2-r^2\sigma} \end{pmatrix} \right] \right\}. \end{aligned} \quad (3)$$

The three Jahn-Teller modes Q_1 , Q_2 , and Q_3 are related to the displacements of oxygen atoms along a , b , and c axes via

$Q_1 = (Q_a + Q_b + Q_c)/\sqrt{3}$, $Q_2 = (Q_b - Q_a)/\sqrt{2}$, and $Q_3 = (Q_a + Q_b - 2Q_c)/\sqrt{6}$. While Q_1 is the usual breathing mode and involves a local volume contraction or expansion, Q_2 and Q_3 modes are typical vibration modes and conserve the local volume.²⁰ $Q_{a,b,c}$ denote the dimensionless lattice distortion along a, b , and c axes. The two corresponding coupling constants are $g_1 = 4\sqrt{3}Ze^2/a_0$ and $g_2 \approx 0.6892(10Dq \times g_1)^{1/2}$. Ze is the effective charge of O ions and a_0 is the lattice constant. Only Q_2 and Q_3 are relevant Jahn-Teller modes to the half-doped $\text{La}_{1/2}\text{Ba}_{1/2}\text{CoO}_3$. It is convenient to define the magnitude Q and angle α through $Q_2 = Q \sin \alpha$ and $Q_3 = Q \cos \alpha$; then $\alpha = 0, 2\pi/3, -2\pi/3$ correspond to the Jahn-Teller distortion axis along c, a , and b axes.

For the effective single-particle Hamiltonian discussed above, the density of states can be easily calculated using the real-space recursion method,²¹ and the Green's function is expressed as

$$G_{m\sigma}^0(\omega) = \frac{b_0^2}{\omega - a_0 - \frac{b_1^2}{\omega - a_1 - \frac{b_2^2}{\omega - a_2 - \frac{b_3^2}{\omega - a_3 - \dots}}}} \quad (4)$$

The recursion coefficients a_i and b_i are computed from the tridiagonalization of the tight-binding Hamiltonian matrix for a given starting orbital. A multiband terminator²² is chosen to close the continuous fractional. We have computed all possible spin state combinations between Co^{3+} and Co^{4+} ions in an enlarged double cell, with 25 levels being calculated for each of the 56 independent orbitals. Our results have been checked for different levels to secure the energy accuracy better than 5 meV. The whole procedure is iterated self-consistently until convergence and the density of states is obtained by $\rho_{ms}(\omega) = -(1/\pi)\text{Im}G_{ms}(\omega)$, which allows us to compute the electron numbers and magnetic moments as well as the total energies of all ordered states.

III. NUMERICAL RESULTS AND DISCUSSIONS

The band-structure parameters of $\text{La}_{1/2}\text{Ba}_{1/2}\text{CoO}_3$ used in this paper come from the cluster model analysis of the photoemission spectra^{4,6} and the *ab initio* local-spin-density-approximation calculations.²³ The Slater-Koster parameters are taken as $(pd\sigma) = -2.0$ eV, $(pd\pi) = 0.922$ eV, $(pp\sigma) = 0.6$ eV, and $(pp\pi) = -0.15$ eV, respectively. The on-site Coulomb repulsion is set as $U = 5.0$ eV. The bare on-site energy of the O- p orbital is taken as the energy reference point $\varepsilon_p = 0$ eV and that of Co- d orbital depends on the Coulomb repulsion, $\varepsilon_d^0 = -28$ eV. The crystal-field splitting and Hund's coupling constant are set as $Dq = 0.16$ eV and $J_H = 0.84$ eV. Its lattice parameters with cubic symmetry are taken as $a = b = c = 3.87$ Å from Ref. 17. When Jahn-Teller distortion is taken into account, the nearest-neighbor O-O hopping integrals are modified by scaling relation $V_{ll'm}$

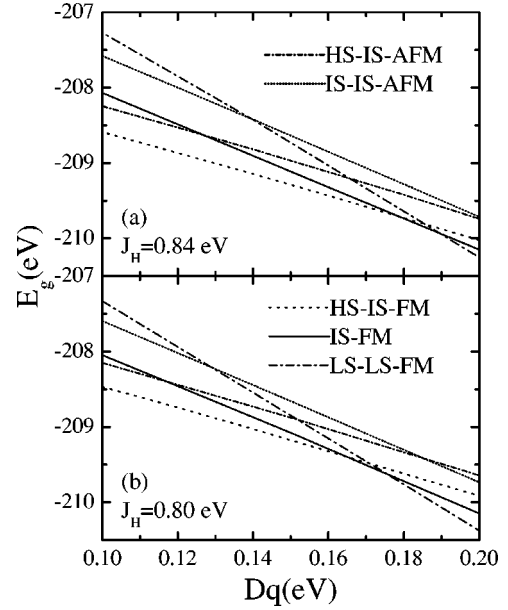


FIG. 1. The energies per double cell of five convergent spin states as a function of the crystal-field splitting Dq . (a) $J_H = 0.84$ eV and (b) $J_H = 0.80$ eV. Other parameters are described in the text.

$= \eta_{ll'm}(\hbar^2/md^2)$, with d denoting the inter-atomic distance; similarly, the hopping integrals between Co- d and O- p follows $V_{ll'm} = \eta_{ll'm}(\hbar^2/md^{3.5})$.²⁴

For reference, we first study the electronic structures and their corresponding energies in the absence of Jahn-Teller distortion. Since both Co^{3+} and Co^{4+} ions have three possible spin-states, there are totally nine nearest-neighbor ferromagnetically ordered states and six nearest-neighbor antiferromagnetically ordered states in a double cell. The self-consistent Hartree-Fock iteration shows that only five of them are convergent; they are HS-IS-FM, charge uniform IS-FM, LS-LS-FM, HS-IS-AFM (antiferromagnetic), and IS-IS-AFM. The energies of these five ordered states are presented in Fig. 1 for two sets of Hund's coupling constant $J_H = 0.80$ and 0.84 eV as a function of crystal-field splitting Dq . The phase diagram for different J_H 's looks the same except for a shift of horizontal coordinate since strong Hund's coupling favors large moment states. The ground state takes consecutively the HS-IS-FM state, the charge uniform IS-FM state, and the LS-LS-FM state as Dq increases. The magnetic moments per primitive cell calculated at $Dq = 0.16$ eV and $J_H = 0.84$ eV are $2.43\mu_B$ for the HS-IS-FM state, $1.78\mu_B$ for the charge uniform IS-FM state, and $0.55\mu_B$ for the LS-LS-FM state, respectively. Although the IS-FM state has the right magnetic moment in comparison with experiment, this state is not stable in the parameter region relevant to the half-doped $\text{La}_{1/2}\text{Ba}_{1/2}\text{CoO}_3$ compound ($Dq = 0.16$ eV).¹⁸ As Jahn-Teller distortion does exist in this half-doped compound, the coupling between the Jahn-Teller active IS Co^{3+} ions, and lattice distortion should not be neglected.

In this paper, we have considered the following three different types of Jahn-Teller distortion modes between the nearest neighbor pairs of CoO_6 octahedra. The $[0,0]$ mode

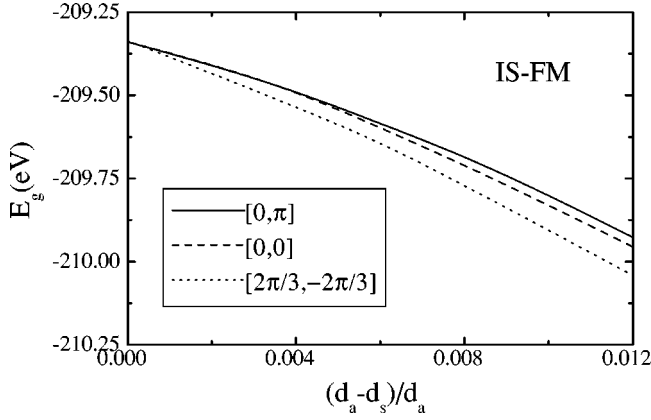


FIG. 2. The energy per double cell of the charge uniform IS-FM state for three different Jahn-Teller modes as a function of distortion size. $Dq=0.16$ eV and $J_H=0.84$ eV. Other parameters are the same as in Fig. 1.

stands for a uniform elongation of all CoO_6 octahedra along the c axis; $[0, \pi]$ for the alternate elongation and contraction of neighboring CoO_6 octahedra along the c axis; and $[2\pi/3, -2\pi/3]$ for the alternate elongation of neighboring CoO_6 octahedra along a and b axes, respectively. The corresponding nearest-neighbor orbital orderings are $[d_{3z^2-r^2}, d_{3z^2-r^2}]$, $[d_{3z^2-r^2}, d_{x^2-y^2}]$, and $[d_{3x^2-r^2}, d_{3y^2-r^2}]$, respectively. Note that all the Jahn-Teller modes discussed above conserve the cell volume. While the first mode involves a symmetry breaking from a cubic lattice to a tetragonal lattice, the other two modes mainly cause cell doubling. It should be emphasized that the third mode in the planar version plays an important role for stabilizing the A -type antiferromagnetic phase in LaMnO_3 .²⁵ Similar to the Mn^{3+} ions in a LaMnO_3 compound, Co^{3+} ions in the IS state also have one electron in the e_g orbitals. One expects that the same Jahn-Teller distortion may also stabilize the IS state. Thus we have calculated the energy of the charge uniform IS state in the presence of the above three Jahn-Teller modes. The results are shown in Fig. 2. Being consistent with the physical intuition, the IS state does lower its energy as a function of $(d_a - d_s)/d_a$, with d_a and d_s denoting the average and short Co-O bond lengths, respectively. However, our result shows that the third Jahn-Teller distortion mode has the strongest impact on the IS state, just as the case in the undoped LaMnO_3 system. The IS state with the third Jahn-Teller mode is characterized by the nearest neighbor $[d_{3x^2-r^2}, d_{3y^2-r^2}]$ orbital ordering. In fact, our conclusion also follows from the Goodenough-Kanamori rule.^{26,27} The rule states that the singly occupied double-degenerate orbitals, such as e_g orbitals, tend to favor ferromagnetic coupling, and the coupling is strongest when the effective hopping between neighboring occupied and unoccupied orbitals is maximized. The $[2\pi/3, -2\pi/3]$ Jahn-Teller mode offers just the desired configuration.

With the above conclusion in mind, we again computed the three most stable spin states in (Dq, J_H) space in the presence of the $[2\pi/3, -2\pi/3]$ Jahn-Teller distortion mode. The phase diagram is presented in Fig. 3, with the distortion

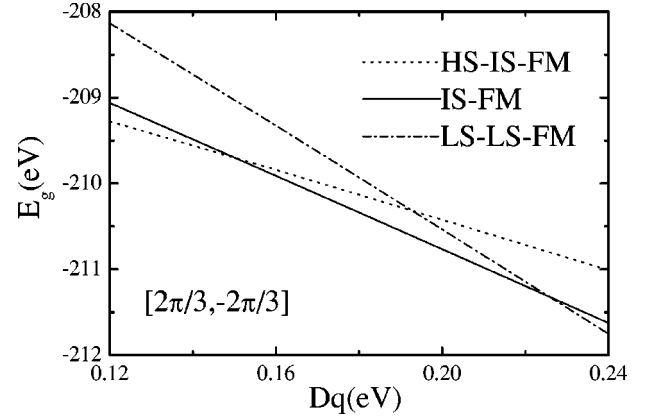


FIG. 3. The energies per double cell of the HS-IS-FM, charge uniform IS-FM, and LS-LS-FM states as a function of Dq for the $[2\pi/3, -2\pi/3]$ Jahn-Teller mode. $(d_a - d_s)/d_a=0.01$ and $J_H=0.84$ eV.

size set as $(d_a - d_s)/d_a=0.01$. Without surprise, the unstable charge uniform IS-FM state (Fig. 1) in the absence of Jahn-Teller distortion is now stabilized in the parameter region relevant to the half-doped compound ($Dq=0.16$ eV). This is because the singly occupied e_g electron benefits from such distortion, while electrons in the HS and LS states do not. Comparing Figs. 3 and 1, our results also indicate that a spin-state transition might occur from the IS state to the HS-IS state as the temperature increases, because the crystal-field splitting usually decreases while Hund's coupling is essentially an atomic quantity which is insensitive to the temperature. The detailed magnetic susceptibility measurement in broader temperature region can be used to check whether such a spin-state transition exists.

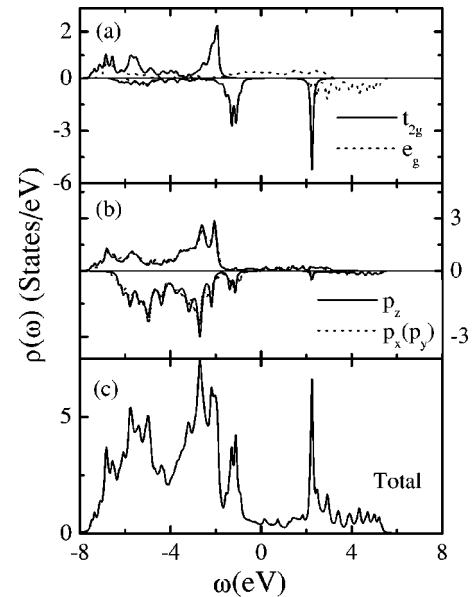


FIG. 4. The densities of states per double cell of the charge uniform IS-FM state for the $[2\pi/3, -2\pi/3]$ Jahn-Teller mode. (a) PDOS of Co- d . (b) PDOS of O- p . (c) Total DOS. $(d_a - d_s)/d_a=0.01$, $Dq=0.16$ eV, and $J_H=0.84$ eV.

In Fig. 4, both partial densities of states (PDOS) and total density of states of the charge uniform IS state of $\text{La}_{1/2}\text{Ba}_{1/2}\text{CoO}_3$ are plotted. The overall profile is quite similar to the IS state of LaCoO_3 .¹¹ The main feature of the valence band comes from the O- p orbitals and the peaks near the Fermi energy ($E_F \equiv 0$) stem from Co- d orbitals. It is shown that the e_g bands of Co ions are quite flat and broad due to the strong itineracy of e_g electrons, so that the total bandwidth is mainly determined by Co- d bands. The electron occupation is 6.65 and the magnetic moment is $1.73\mu_B$ for $(d_a - d_s)/d_a = 0.01$. This state is metallic, as a finite density of states exists at the Fermi energy, which is consistent with the experimental measurements.^{15,16} Just like $\text{La}_{1-x}\text{Ba}_x\text{MnO}_3$ -based giant magnetoresistance materials, $\text{La}_{1/2}\text{Ba}_{1/2}\text{CoO}_3$ is also a half-metal.²⁸

IV. CONCLUSION

In summary, various spin states of Co^{3+} and Co^{4+} ions of $\text{La}_{1/2}\text{Ba}_{1/2}\text{CoO}_3$ are calculated using the Hartree-Fock approximation and the real-space recursion method. The roles of different Jahn-Teller modes on these spin states are ex-

plored. Our results show that only HS-IS-FM, charge uniform IS-FM, and LS-LS-FM states can be the ground state. The charge uniform IS-FM state is unstable in the parameter region relevant to half-doped compounds if the Jahn-Teller distortion is absent. However, the IS Co^{3+} ions are strongly coupled to the Jahn-Teller modes, and are indeed stabilized by a reasonable size of distortion. It is also seen in our calculation that the $[2\pi/3, -2\pi/3]$ Jahn-Teller mode with $d_{3x^2-r^2}/d_{3y^2-r^2}$ orbital ordering is the most favorable one, which appears to be inconsistent with the experimental observation though it agrees with the general Goodenough-Kanamori rule. Note that previous experiments^{29,30} only observed a local tetragonal distortion, which is not in conflict with our conclusion.

ACKNOWLEDGMENTS

The work was supported by a CRCG grant at the University of Hong Kong, the NSFC of China under Grant Nos. 19767202, 10021001, and 0025419, and the '973 Program' of NSTC of China under Grant No. 199806.

-
- ¹R. von Helmolt, J. Wecker, B. Holzapfel, L. Schultz, and K. Samwer, *Phys. Rev. Lett.* **71**, 2331 (1993).
²M. McCormack, S. Jin, T.H. Tiefl, R.M. Fleming, J.M. Phillips, and R. Ramesh, *Appl. Phys. Lett.* **64**, 3045 (1994).
³G.H. Jonker, *J. Appl. Phys.* **37**, 1424 (1966).
⁴P.M. Raccah and J.B. Goodenough, *Phys. Rev.* **155**, 932 (1967).
⁵K. Asai, P. Gehring, H. Chou, and G. Shirane, *Phys. Rev. B* **40**, 10 982 (1989).
⁶M.A. Senaris-Rodriguez and J.B. Goodenough, *J. Solid State Chem.* **116**, 224 (1995).
⁷S. Yamaguchi, Y. Okimoto, H. Taniguchi, and Y. Tokura, *Phys. Rev. B* **53**, R2926 (1996).
⁸T. Saitoh, T. Mizokawa, A. Fujimori, M. Abbate, Y. Takeda, and M. Takano, *Phys. Rev. B* **55**, 4257 (1997).
⁹I. Solovyev, N. Hamada, and K. Terakura, *Phys. Rev. B* **53**, 7158 (1996).
¹⁰M.A. Korotin, S.Yu. Ezhov, I.V. Solovyev, V.I. Anisimov, D.I. Khomskii, and G.A. Sawatzky, *Phys. Rev. B* **54**, 5309 (1996).
¹¹M. Zhuang, W. Zhang, and N. Ming, *Phys. Rev. B* **57**, 10 705 (1997).
¹²D. Louca, J.L. Sarrao, J.D. Thompson, H. Roder, and G.H. Kwei, *Phys. Rev. B* **60**, 10 378 (1999).
¹³V.G. Sathe, A.V. Pimpale, V. Siruguri, and S.K. Paranjpe, *J. Phys.: Condens. Matter* **8**, 3889 (1996).
¹⁴H. Taguchi, M. Shirnada, and M. Koizumi, *Mater. Res. Bull.* **13**, 1225 (1978); *J. Solid State Chem.* **29**, 221 (1979).
¹⁵Y. Moritomo, M. Takeo, X.J. Liu, T. Akimoto, and A. Nakamura, *Phys. Rev. B* **58**, R13 334 (1998).
¹⁶I.O. Troyanchuk, N.V. Kasper, D.D. Khalyavin, H. Szymczak, R. Szymczak, and M. Baran, *Phys. Rev. B* **58**, 2418 (1998).
¹⁷F. Fauth, E. Suard, and V. Caignaert, *Phys. Rev. B* **65**, 060401 (2002).
¹⁸M. Zhuang, W. Zhang, T. Zhou, and N. Ming, *Phys. Lett. A* **255**, 354 (1999).
¹⁹T. Mizokawa and A. Fujimori, *Phys. Rev. B* **54**, 5368 (1996).
²⁰K.I. Kugel and D.I. Khomskii, *Sov. Phys. Usp.* **25**, 231 (1982).
²¹V. Heine, R. Haydock, and M. J. Kelly, in *Solid State Physics: Advances in Research and Applications*, edited by H. Ehrenreich, F. Seitz, and D. Turnbull (Academic, New York, 1980), Vol. 35, p. 215.
²²R. Haydock and C.M.M. Nex, *J. Phys. C* **17**, 4783 (1984).
²³D.D. Sarma, N. Shanthi, S.R. Barman, N. Hamada, H. Sawada, and K. Terakura, *Phys. Rev. Lett.* **75**, 1126 (1995).
²⁴W. A. Harrison, in *Electronic Structure and the Properties of Solids* (Freeman, San Francisco, 1980).
²⁵Y. Murakami, J.P. Hill, D. Gibbs, M. Blume, I. Koyama, M. Tanaka, H. Kawata, T. Arima, Y. Tokura, K. Hirota, and Y. Endoh, *Phys. Rev. Lett.* **81**, 582 (1998).
²⁶J.B. Goodenough, *Phys. Rev.* **100**, 564 (1955).
²⁷J. Kanamori, *J. Phys. Chem. Solids* **10**, 87 (1959).
²⁸W.E. Pickett and D.J. Singh, *Phys. Rev. B* **53**, 1146 (1996).
²⁹Z. Wang and J. Zhang, *Phys. Rev. B* **54**, 1153 (1996).
³⁰S. Yamaguchi, Y. Okimoto, and Y. Tokura, *Phys. Rev. B* **55**, R8666 (1997).